

DEVELOPMENT OF A TRAJECTORY PLANNING ALGORITHM FOR A 4-DOF ROCKBREAKER BASED ON HYDRAULIC FLOW RATE LIMITS

Louis-Francis Tremblay, Marc Arsenault, Meysar Zeinali
Bharti School of Engineering, Laurentian University, Sudbury, ON, Canada
Email: marc.arsenault@laurentian.ca

ABSTRACT

In this paper, a novel trajectory planning methodology is proposed for use within a semi-automated hydraulic rockbreaker system. The objective of the proposed method is to minimize the trajectory duration while hydraulic fluid flow rate limits are respected. Within the trajectory planning methodology, a point-to-point path planning approach based on the decoupling of the motion of the rockbreaker's first joint is compared to an alternative approach based on Cartesian straight-line motion. Each of these path types are parameterized as a function of time based on an imposed trajectory profile that ensures smooth rockbreaker motions. A constrained nonlinear optimization problem is formulated and solved with the trajectory duration as the objective function while constraints are applied to ensure that flow rate limits through the rockbreaker's proportional valves and hydraulic pump are not exceeded. The proposed methodology is successfully implemented to compute a set of representative trajectories with the path planning approach based on the decoupling of the motion of the rockbreaker's first joint consistently producing shorter trajectory durations.

Keywords: rockbreaker; hydraulic robot; path planning; trajectory planning; mining robotics; mining automation.

DÉVELOPPEMENT D'UN ALGORITHME DE PLANIFICATION DE TRAJECTOIRES EN FONCTION DES LIMITES DE DÉBITS HYDRAULIQUES POUR UN BRISE-ROCHE À 4 DDL

RÉSUMÉ

Dans cet article, une méthode novatrice est proposée pour la planification de trajectoires d'un brise-roche hydraulique semi-automatisé. L'objectif visé est de minimiser la durée des trajectoires tout en assurant le respect des limites qui s'appliquent aux débits de fluide hydraulique. En ce sens, les trajectoires point à point fondées sur le découplage du mouvement de rotation associé au premier axe du brise-roche sont comparées aux trajectoires en ligne droite dans l'espace cartésien. Chacun de ces types de trajectoires sont paramétrisés en fonction du temps selon un profil imposé qui assure un mouvement graduel et continu du brise-roche. Un problème d'optimisation sous contraintes non-linéaire est formulé et résolu en utilisant la durée de trajectoire comme fonction objective, les contraintes cherchant à assurer que les limites de débits de fluide hydraulique passant par les soupapes et la pompe soient respectées. La méthodologie proposée est validée en l'appliquant à un ensemble de trajectoires représentatives. Il est observé que l'approche basée sur le découplage du mouvement du brise-roche produit des trajectoires de durées plus courtes.

Mots-clés : brise-roche ; robot hydraulique ; planification de trajectoires ; robotique minière ; automatisation des processus miniers.

1. INTRODUCTION

A rockbreaker is a hydraulically driven machine used in the mining industry whose purpose is to break large pieces of ore. A typical operation is shown in Fig. 1(a) where the grizzly acts as a filter through which ore must pass. Benefits related to the automation of rockbreakers include increases to workplace safety, efficiency and productivity as well as decreases in operating and maintenance costs [1–4]. Automation also increases the ease of use of rockbreakers and reduces the need for operator training [5]. While teleoperated rockbreakers achieve some of these benefits, they are challenged by limited operator visibility, depth perception and system latency [1, 6]. Meanwhile, the full automation of a rockbreaker is impeded by the requirement of sensing oversize rock locations and shapes to determine the optimal breaker tip pose for breaking ore [1]. This paper proposes a semi-automation approach based on the following procedure:

1. The operator specifies an oversize rock location using a graphical user interface.
2. The rockbreaker automatically moves to the specified location above the oversize rock in two sequential steps:
 - i) Motion of the breaker tip along a vertical line to bring it to the work plane.
 - ii) Horizontal trajectory of the breaker tip within the work plane to bring it to the specified location.
3. The operator breaks the rock through a teleoperation interface.

The work plane (Fig. 1(a)) is located above the largest piece of ore on the grizzly. The proposed approach, similar to those described in [1, 7], allows the operator to drive multiple rockbreakers simultaneously. Trajectory planning, one of the main components of rockbreaker semi-automation, is the focus of this work.

A rockbreaker is a hydraulically actuated four-degree-of-freedom (4-DoF) robot. While robot trajectory planning has been extensively researched [8, 9], the use of hydraulic actuation is accompanied by specific additional requirements. For instance, trajectories must consider hydraulic fluid pressure and flow rate limits. As such, separate research exists dealing with the trajectory planning of such machines [10]. Much of the existing work deals with hydraulic excavators [2, 11–14], which share many similarities with rockbreakers. A simplified approach to motion planning using pre-programmed scripts based on common excavator motions is proposed in [11]. Straight-line paths in Cartesian space parameterized using trapezoidal velocity profiles are used in [2]. The resulting trajectories are not smooth nor optimal and flow rate limitations are not explicitly considered. Optimized excavator trajectories that seek to minimize trajectory duration and

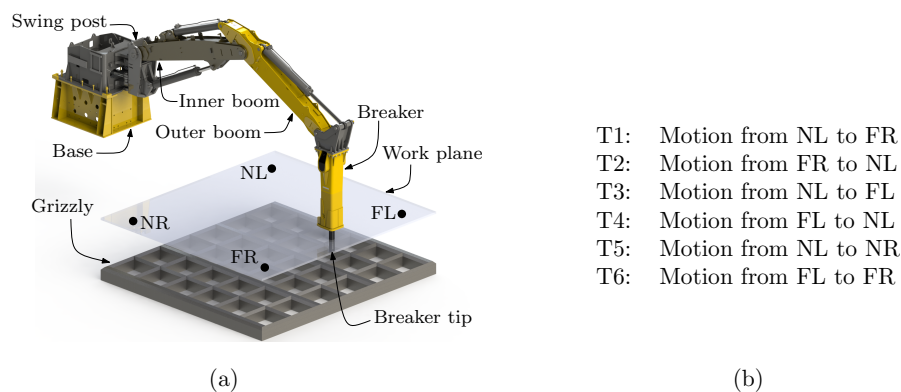


Fig. 1. (a) Typical rockbreaker installation with grizzly used in underground mining operations and (b) definition of validation trajectories.

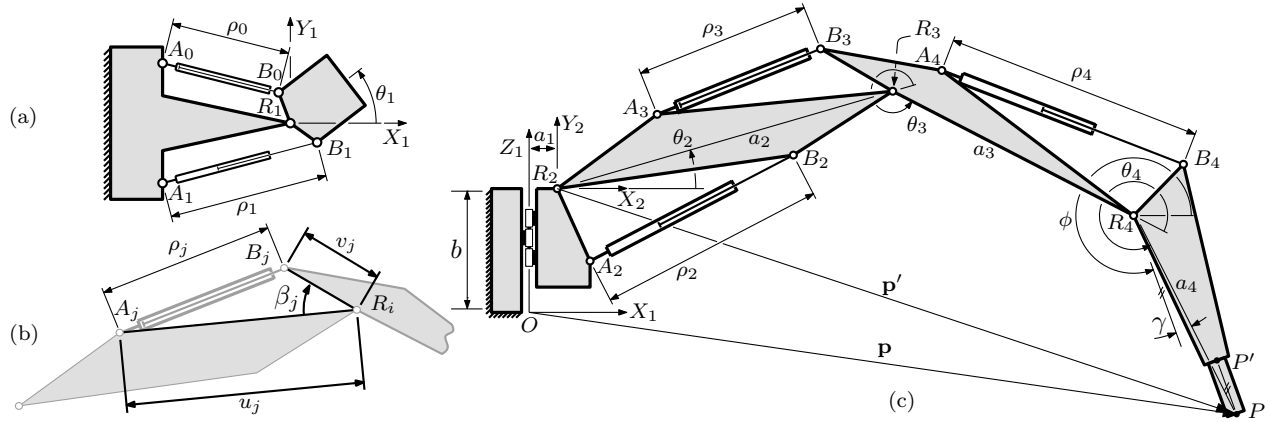


Fig. 2. Schematic representation of rockbreaker with parameter definitions: (a) Top view of base and swing post, (b) detailed side view of a typical joint and (c) side view of complete rockbreaker

joint torques are proposed in [12]. However, the excavator's motion in Cartesian space, of critical importance for underground mining applications, is not directly prescribed. This issue also exists in [13] where time-optimal trajectories are found by optimizing the motion between way-points using the virtual motion camouflage approach. Flow rate limitations are imposed by setting limits on the angular motion of the excavator's revolute joints, which represents an overly conservative approach. The same approach is used in [7] to develop a library of optimized trajectories for forwarder cranes using B-splines paths. Meanwhile, straight line Cartesian trajectories are developed from velocity profiles with sinusoidal ramp-up/down segments in [14] while applying constant Cartesian velocity and acceleration limits. Finally, a global path planner based on pre-programmed way-points to generate smooth rockbreaker trajectories while satisfying flow rate limits is proposed in [1]. However, few details are provided on the implementation of the proposed approach.

Trajectory planning may be considered as the combination of two tasks: path planning and time parameterization [15]. The method proposed herein addresses each of these tasks sequentially. Predictable paths in Cartesian space are defined either as straight lines or with decoupled swing joint motion, allowing for path validation in cluttered underground environments. The time parameterization of the paths is then done using smooth profiles while minimizing trajectory duration. This is accomplished while taking into account hydraulic pump and valve flow rate limits and their configuration-dependent impact on joint velocities.

2. KINEMATIC ANALYSIS OF THE ROCKBREAKER

The rockbreaker is shown schematically in Fig. 2, where link lengths a_i ($i = 1, 2, 3, 4$) are measured between the axes of revolute joints R_i and R_{i+1} (though a_4 is measured from R_4 to the breaker tip P). The revolute joints, with angular displacements θ_i , are driven by hydraulic prismatic actuators of length ρ_j ($j = 0, 1, \dots, 4$) acting between the actuator body (A_j) and rod (B_j) pin connections. In the case of R_1 , two actuators (ρ_0 and ρ_1) are used in parallel. The hydraulic actuators and revolute joints are mechanically limited such that $\rho_{j_{\min}} \leq \rho_j \leq \rho_{j_{\max}}$ and $\theta_{i_{\min}} \leq \theta_i \leq \theta_{i_{\max}}$. The breaker's pose is described by the position $\mathbf{p} = [x, y, z]^T$ of point P combined with its orientation ϕ . The latter is measured from the X_2 axis of frame $X_2Y_2Z_2$, attached to the swing post, to the axis of the breaker (*i.e.* the line passing through points P' and P). The hydraulic actuators are controlled through proportional valves and the rates of change of their lengths, *i.e.* $\dot{\rho}_j$, are subject to valve ($Q_{i_{\max}}$) and pump ($Q_{p_{\max}}$) flow rate limits (the same valve controls ρ_0 and ρ_1).

The direct kinematic problem (DKP) computes the pose $\mathbf{x} = [\mathbf{p}^T, \phi]^T$ for given ρ_j . One has:

$$\beta_i = \cos^{-1} \left(\frac{u_i^2 + v_i^2 - \rho_j^2}{2u_i v_i} \right) \quad (1)$$

where only one of ρ_0 or ρ_1 is needed to find β_1 . Afterwards, θ_i may be obtained from β_i as

$$\theta_i = \delta_i \beta_i + \varepsilon_i \quad (2)$$

where ε_i is an angular offset based on the system's geometry and δ_i is the i^{th} element of $\delta = [1, 1, -1, -1]^T$. With $c_i = \cos(\theta_i)$, $s_{ij} = \sin(\theta_i + \theta_j)$, etc., the rockbreaker's pose is finally obtained as

$$\mathbf{x} = \begin{bmatrix} \mathbf{p} \\ \phi \end{bmatrix} = \begin{bmatrix} c_1(a_1 + a_2c_2 + a_3c_{23} + a_4c_{234}) \\ s_1(a_1 + a_2c_2 + a_3c_{23} + a_4c_{234}) \\ b + a_2s_2 + a_3s_{23} + a_4s_{234} \\ \theta_2 + \theta_3 + \theta_4 - \gamma \end{bmatrix} \quad (3)$$

In order to solve the inverse kinematic problem (IKP), the swing post's orientation is first obtained as¹ $\theta_1 = \text{atan2}(y, x)$. Afterwards θ_2 , θ_3 and θ_4 are found by considering the inner boom, outer boom and breaker as the links of a 3-DoF planar 3R robot whose IKP yields up to two solutions [16]. The corresponding actuator lengths (*i.e.* ρ_j) may then be found from Eqs. (1) and (2).

A relationship between the actuator and Cartesian velocities is obtained as $\dot{\mathbf{x}} = \mathbf{J}_\theta \mathbf{J}_\beta \mathbf{J}_\rho \dot{\rho}$ with

$$\mathbf{J}_\theta = \begin{bmatrix} -s_1 \alpha & -c_1(a_2s_2 + a_3s_{23} + a_4s_{234}) & -c_1(a_3s_{23} + a_4s_{234}) & -c_1(a_4s_{234}) \\ c_1 \alpha & -s_1(a_2s_2 + a_3s_{23} + a_4s_{234}) & -s_1(a_3s_{23} + a_4s_{234}) & -s_1(a_4s_{234}) \\ 0 & a_2c_2 + a_3c_{23} + a_4c_{234} & a_3c_{23} + a_4c_{234} & a_4c_{234} \\ 0 & 1 & 1 & 1 \end{bmatrix} \quad (4)$$

$$\mathbf{J}_\beta = \begin{bmatrix} \delta_1/2 & \delta_1/2 & 0 & 0 & 0 \\ 0 & 0 & \delta_2 & 0 & 0 \\ 0 & 0 & 0 & \delta_3 & 0 \\ 0 & 0 & 0 & 0 & \delta_4 \end{bmatrix}, \quad \mathbf{J}_\rho = \begin{bmatrix} J_{\rho_0} & & & & \\ & J_{\rho_1} & & & \\ & & \ddots & & \\ & & & & J_{\rho_4} \end{bmatrix}, \quad J_{\rho_j} = \frac{\rho_j}{u_j v_j \sin \beta_j} \quad (5)$$

where $\dot{\rho} = [\dot{\rho}_0, \dot{\rho}_1, \dot{\rho}_2, \dot{\rho}_3, \dot{\rho}_4]^T$ and $\alpha = a_1 + a_2c_2 + a_3c_{23} + a_4c_{234}$. One also has $\dot{\rho} = \mathbf{J}_\rho^{-1} \mathbf{J}_\beta^* \mathbf{J}_\theta^{-1} \dot{\mathbf{x}}$ with

$$\mathbf{J}_\beta^* = \begin{bmatrix} 1/J_{\beta_0} & 0 & 0 & 0 & 0 \\ 1/J_{\beta_1} & 0 & 0 & 0 & 0 \\ 0 & 1/J_{\beta_2} & 0 & 0 & 0 \\ 0 & 0 & 1/J_{\beta_3} & 0 & 0 \\ 0 & 0 & 0 & 1/J_{\beta_4} & 0 \end{bmatrix} \quad (6)$$

An example of the rockbreaker's workspace, using the parameter values listed in Table 1, is illustrated in Fig. 3 for the case where $\theta_1 = 0$. The three-dimensional workspace is obtained by sweeping the region illustrated in Fig. 3 about the Z_1 axis over the range $\theta_{1\min} \leq \theta_1 \leq \theta_{1\max}$. The subset of the workspace where the rockbreaker may operate with its breaker in a vertical orientation (*i.e.* $\phi = 270^\circ$) is also shown.

In order to verify the valve and pump flow rate limits, the required flow rates for prescribed actuator velocities must be computed. For a given $\dot{\rho}$, the valve flow rates are obtained as $\mathbf{Q}_v = \mathbf{J}_v |\dot{\rho}|$ with

$$\mathbf{J}_v = \begin{bmatrix} A_0 & A_1 & 0 & 0 & 0 \\ 0 & 0 & A_2 & 0 & 0 \\ 0 & 0 & 0 & A_3 & 0 \\ 0 & 0 & 0 & 0 & A_4 \end{bmatrix} \quad (7)$$

¹Note: "atan2" is the quadrant corrected arctangent (or four-quadrant inverse tangent) function.

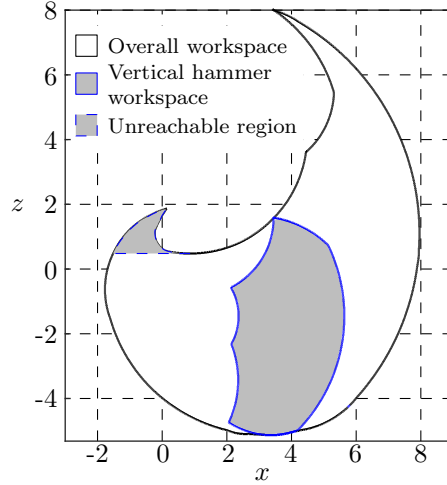


Fig. 3. Two-dimensional slice of the rockbreaker's workspace.

where $\mathbf{Q}_v = [Q_1, Q_2, Q_3, Q_4]^T$ and $|\dot{\rho}| = [|\dot{\rho}_0|, |\dot{\rho}_1|, \dots, |\dot{\rho}_4|]^T$. In Eq. (7), A_j is the area of the j -th actuator surface on which the hydraulic fluid is acting. Specifically, A_j is equal to the area A_{blind_j} of the j th actuator piston's blind side when $\dot{\rho}_j > 0$ while it is equal to the area A_{rod_j} of the rod side when $\dot{\rho}_j < 0$ (numerical values used for the validation of the proposed methodology are provided in Section 4). Combined with the required pump flow $Q_p = \sum_i Q_i$, this yields the total flow rate vector $\mathbf{Q} = [Q_1, Q_2, Q_3, Q_4, Q_p]^T$.

3. DESCRIPTION OF THE TRAJECTORY PLANNING METHODOLOGY

The semi-automated rockbreaker requires trajectories to be defined between initial and final poses. The initial pose ($\mathbf{x} = [\mathbf{p}_I^T, \phi_I]^T$) is obtained from the DKP based on measured actuator lengths. The final position \mathbf{p}_F is specified by the operator based on the location of the ore to be broken while the final orientation ϕ_F is calculated according to Section 3.1. While the path between the initial and final poses is not critical, it must be predictable to allow checking for collisions between the rockbreaker and its environment. In fact, given the serious consequences of underground collisions between the rockbreaker and its surroundings as well as the environmental challenges associated with the use of sensors to detect obstacles in real-time, the proposed approach seeks to confirm that trajectories are collision-free prior to any rockbreaker motion. In this way, trajectory planning is not performed in real-time.

As previously mentioned, trajectory planning is a combination of path planning and time parameterization [15]. In terms of path planning, decoupled swing joint motion (DSJM) and Cartesian straight-line motion (CSLM) paths are considered. Meanwhile, the time parameterization of the paths will seek to minimize the total trajectory duration subject to valve and pump flow rate limits.

3.1. Calculation of the Final Pose Orientation

While the operator specifies \mathbf{p}_F , ϕ_F is found based on the objective of keeping the breaker orientation as vertical as possible² to facilitate the breaking of ore. The feasibility of a vertical breaker orientation is first verified by solving the IKP with \mathbf{p}_F and $\phi_F = 270$ degrees as inputs and verifying if $\rho_{j_{\min}} \leq \rho_j \leq \rho_{j_{\max}}$. If a vertical breaker orientation is not feasible, ϕ_F is found from the following minimization

$$\min_{\theta_2, \theta_3, \theta_4} (\theta_2 + \theta_3 + \theta_4 - \gamma - 270)^2 \quad (8)$$

²It may be seen in Fig. 3 that vertical breaker orientations are not always feasible.

where $\phi = \theta_2 + \theta_3 + \theta_4 - \gamma$ and angles are expressed in degrees. Intuitively, the solution to this problem corresponds to a situation where $\theta_i = \theta_{i_{\min}}$ or $\theta_i = \theta_{i_{\max}}$ for $i = 2, 3$ or 4 (otherwise, $\phi_F = 270$ degrees would be feasible). Based on this observation, ϕ_F may be found using the following procedure for $\mathbf{p} = \mathbf{p}_F$:

1. Set $\theta_k = \theta_{k_{\min}}$ or $\theta_k = \theta_{k_{\max}}$ ($k = 2, 3$ or 4).
2. Given \mathbf{p} , solve the IKP for the remaining (unconstrained) revolute joint angles (*i.e.* θ_i with $i \neq k$) and verify their feasibility (*i.e.* $\theta_{i_{\min}} \leq \theta_i \leq \theta_{i_{\max}}$).
3. For all feasible solutions, add $\phi = \theta_2 + \theta_3 + \theta_4 - \gamma$ to a list of possible minimum values.
4. Repeat steps 1 through 3 for each limit ($\theta_{k_{\min}}$ and $\theta_{k_{\max}}$) of each joint ($k = 2, 3, 4$) which generates a maximum of 12 candidate ϕ values.
5. From the generated list of ϕ values, identify the minimum ϕ_{\min} and maximum ϕ_{\max} such that the range of admissible breaker orientations is $\phi_{\min} \leq \phi \leq \phi_{\max}$.

If no feasible value of ϕ is found for a given \mathbf{p} , the desired position of the rockbreaker is outside its workspace and cannot be reached. Otherwise, ϕ_F is set to either ϕ_{\min} or ϕ_{\max} (*i.e.* the closest to vertical).

3.2. DSJM Path Planning

In the DSJM case, the path of the swing joint (θ_1) is planned independently of the motion within the X_2Y_2 plane (θ_2 , θ_2 and θ_3). Referring to Fig. 3, the benefit of the DSJM approach is that it generates paths in the horizontal work plane that are guaranteed to be located within the workspace so long as $x \gtrsim 0$ (which is typical in real-world applications). However, the breaker tip is not guaranteed to remain within a rectangular prism extending vertically above the grizzly, which increases the probability of collisions with surrounding walls, etc. Given $\mathbf{p}_I = [x_I, y_I, z_I]^T$ and $\mathbf{p}_F = [x_F, y_F, z_F]^T$, the corresponding swing joint angles are $\theta_{1_I} = \text{atan2}(y_I, x_I)$ and $\theta_{1_F} = \text{atan2}(y_F, x_F)$. The DSJM-based path then becomes

$$\theta_1 = \theta_{1_I} + \sigma \cdot (\theta_{1_F} - \theta_{1_I}) \quad (9)$$

$$\mathbf{p}' = \mathbf{p}'_I + \sigma \cdot (\mathbf{p}'_F - \mathbf{p}'_I) \quad (10)$$

$$\phi = \phi_I + \sigma \cdot (\phi_F - \phi_I) \quad (11)$$

where \mathbf{p}' , \mathbf{p}'_I and \mathbf{p}'_F correspond to \mathbf{p} , \mathbf{p}_I and \mathbf{p}_F expressed in frame $X_2Y_2Z_2$. Moreover, $\sigma \in [0, 1]$ is a monotonically increasing variable whose time parameterization remains to be determined. Eqs. (9) – (11) may subsequently be converted into corresponding actuator lengths ρ_j with the IKP.

3.3. CSLM Path Planning

In this case, the breaker tip travels along a straight line while its orientation is changing. CSLM paths guarantee that the breaker tip remains above the grizzly at all times, which decreases the probability of collisions. Given \mathbf{p}_I , \mathbf{p}_F , ϕ_I and ϕ_F , the CSLM-generated path is expressed by Eq. (11) combined with

$$\mathbf{p} = \mathbf{p}_I + \sigma \cdot (\mathbf{p}_F - \mathbf{p}_I) \quad (12)$$

Once again, corresponding actuator lengths are obtained with the IKP. While the feasibility of CSLM paths are not guaranteed given the non-convexity of the rockbreaker's workspace, in most cases this is not an issue and would a symptom of a poor installation.

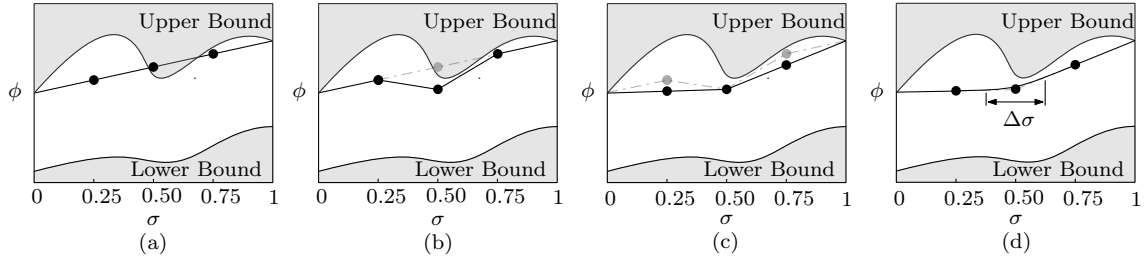


Fig. 4. Example of an initially non-feasible $\phi(\sigma)$ trajectory that is subjected to quarter point shifts in order to render it feasible

3.4. Path Validation

While \mathbf{x}_I and \mathbf{x}_F have been verified to be feasible, the same cannot be said for the path between them. The path feasibility can be verified by first computing \mathbf{p} for a given σ using Eq. (12) (CSLM case) or Eqs. (9) and (10) combined with $\mathbf{p} = \mathbf{a}_1 + \mathbf{R}_2^1 \mathbf{p}'$ where \mathbf{R}_2^1 is a rotation matrix dependent on θ_1 bringing frame $X_1Y_1Z_1$ parallel to $X_2Y_2Z_2$ and \mathbf{a}_1 is the position of the origin of frame $X_2Y_2Z_2$ expressed in $X_1Y_1Z_1$ (DSJM case). Afterwards, ϕ_{\min} and ϕ_{\max} are calculated for \mathbf{p} according to Section 3.1. If ϕ_{\min} and ϕ_{\max} exist, the breaker tip position \mathbf{p} is feasible (this should always be the case for the DSJM path so long as it remains within the horizontal work plane). The pose will be feasible if ϕ obtained from Eq. (11) satisfies $\phi_{\min} \leq \phi \leq \phi_{\max}$. By repeating these verifications for $\sigma \in [0, 1]$, the feasibility of the DSJM and CSLM paths are known. If non-feasible breaker orientations are found along either path, Eq. (11) must be modified. Plotting ϕ_{\min} and ϕ_{\max} as a function of σ defines a region of admissible breaker orientations within the $\sigma - \phi$ plane (Fig. 4). If the path described by Eq. (11) is not feasible, the corresponding line in the $\sigma - \phi$ plane will not remain within this region (Fig. 4(a)). By shifting the “quarter points” of the path defined by Eq. (11), *i.e.* $\sigma_q = 0.25q$ with $q = 1, 2, 3$, it may be guided into the feasible region. Each σ_q for which $\phi(\sigma_q) \notin [\phi_{\min_q}, \phi_{\max_q}]$ is first shifted into the admissible region (Fig. 4(b)). Any remaining σ_q are then modified as required to minimize the number of line segments defining the $\phi(\sigma)$ function (Fig. 4(c)). Finally, polynomial blends are added to smooth any corners created in the process of shifting the quarter points (Fig. 4(d)). The modified $\phi(\sigma)$ function is thus piecewise defined as a combination of straight line and polynomial blend segments. The latter are defined using 5th-order polynomials of width $\Delta\sigma = 0.025$ whose coefficients are chosen based on boundary conditions at each end of the blend region corresponding to the known breaker orientations, the required $d\phi/d\sigma$ (corresponding to the slopes of the two meeting line segments) and $d^2\phi/d\sigma^2 = 0$.

3.5. Time Parameterization of the DSJM and CSLM Paths

The time parameterization of the DSJM and CSLM paths consists of defining $\sigma(t)$. The proposed profile at the velocity level, *i.e.* $\dot{\sigma}(t)$, is chosen to consist of smooth polynomial ramp-up/-down segments to/from a segment of constant velocity $\dot{\sigma}_c$ (refer to Fig. 5(a)). The total change in σ over the trajectory is $d_f = 2d_r + d_c = 1$ where d_r and d_c result from the ramp-up/-down segments and the constant velocity segment, respectively. Given the ramp-up/-down duration t_r and the total trajectory duration t_f , one also has $d_c = (t_f - 2t_r)\dot{\sigma}_c$. The ramp-up segment of the trajectory is defined as

$$\sigma(t) = h_0 + h_1t + h_2t^2 + h_3t^3 + h_4t^4 + h_5t^5, \quad t \in [0, t_r] \quad (13)$$

and it is simply mirrored to obtain the ramp-down segment (Fig. 5(a)). The polynomial's coefficients are obtained from the following boundary conditions

$$\sigma(0) = 0, \quad \sigma(t_r) = d_r, \quad \dot{\sigma}(t_r) = \dot{\sigma}_c, \quad \dot{\sigma}(0) = \ddot{\sigma}(0) = \ddot{\sigma}(t_r) = 0 \quad (14)$$

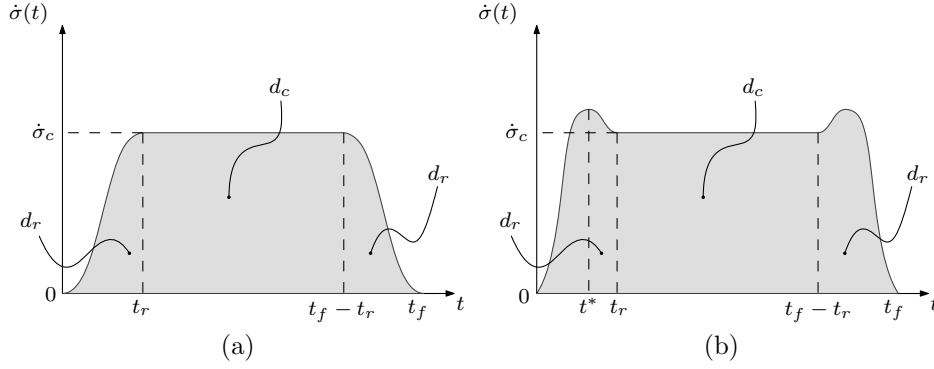


Fig. 5. Trajectory profile for $\dot{\sigma}$: (a) Acceptable trajectory profile and (b) undesired trajectory profile due to the presence of a velocity overshoot

by solving the following system for \mathbf{h} where \mathbf{A} is non-singular so long as $t_r > 0$

$$\mathbf{c} = \begin{bmatrix} \sigma(0) \\ \dot{\sigma}(0) \\ \ddot{\sigma}(0) \\ \sigma(t_r) \\ \dot{\sigma}(t_r) \\ \ddot{\sigma}(t_r) \end{bmatrix} = \begin{bmatrix} 1 & 0 & 0 & 0 & 0 & 0 \\ 0 & 1 & 0 & 0 & 0 & 0 \\ 0 & 0 & 2 & 0 & 0 & 0 \\ 1 & t_r & t_r^2 & t_r^3 & t_r^4 & t_r^5 \\ 0 & 1 & 2t_r & 3t_r^2 & 4t_r^3 & 5t_r^4 \\ 0 & 0 & 2 & 6t_r & 12t_r^2 & 20t_r^3 \end{bmatrix} \begin{bmatrix} h_0 \\ h_1 \\ h_2 \\ h_3 \\ h_4 \\ h_5 \end{bmatrix} = \mathbf{A}\mathbf{h} \quad (15)$$

Prior to solving for the polynomial's coefficients, t_r , d_r and $\dot{\sigma}_c$ are determined from a constrained minimization of the trajectory duration, *i.e.*

$$\min_{\mathbf{y}} t_f = \frac{1 - 2d_r}{\dot{\sigma}_c} + 2t_r \quad (16)$$

where $\mathbf{y} = [t_r, d_r, \dot{\sigma}_c]^T$ is the design vector and the following constraints are applied

$$\mathcal{C}_1: d_r \leq 0.5, \quad \mathcal{C}_2: t_{r\min} \leq t_r \leq 0.5t_f, \quad \mathcal{C}_3: \ddot{\sigma}(0) \geq 0 \text{ and } \ddot{\sigma}(t_r) \leq 0, \quad \mathcal{C}_4: \mathbf{Q}(t) \leq \mathbf{Q}_{\min} \text{ for } 0 \leq t \leq t_f$$

The optimization problem is solved using sequential quadratic programming. \mathcal{C}_1 as well as the upper bound of \mathcal{C}_2 represent natural limits on d_r and t_r , respectively, while the lower bound of \mathcal{C}_2 is an empirically chosen constant parameter value selected to provide adequate time for the rockbreaker to reach its cruising speed (or for $\dot{\sigma}$ to reach $\dot{\sigma}_c$). This is an indirect approach to ensuring acceptable rockbreaker accelerations which translates to acceptable limits on the hydraulic fluid pressures. This approach, an equivalent version of which was used in [7], is justified given that a rockbreaker's hydraulic actuators mostly work to offset its weight [17] and break ore (the latter of which is outside the scope of this work). Meanwhile, \mathcal{C}_3 ensures that $0 \leq \dot{\sigma}(t) \leq \dot{\sigma}_c$ when $t \in [0, t_r]$. Given that $\ddot{\sigma}(0) = \ddot{\sigma}(t_r) = 0$, problematic situations such as the one illustrated in Fig. 5(b) would require $\dot{\sigma}(t)$ to change sign with the time interval $0 < t < t_r$. From observation, this may only occur if $\ddot{\sigma}(t)$ undergoes two sign changes within the same time interval. Given that \mathcal{C}_3 requires the signs of $\ddot{\sigma}(0)$ and $\ddot{\sigma}(t_r)$ to be different combined with the fact that $\ddot{\sigma}(t)$ is a quadratic polynomial, this situation is avoided. Finally, \mathcal{C}_4 requires that the valve and pump flow rates not exceed the limits described within \mathbf{Q}_{\min} (the “ \leq ” operator is interpreted separately for each of the pairs of elements within \mathbf{Q} and \mathbf{Q}_{\min}). An additional constraint is added to the optimization problem for the DSJM case. From Section 2, it is found that $Q_1 = A_0|\dot{\rho}_0| + A_1|\dot{\rho}_1|$ and $\dot{\rho}_j = (2u_jv_j \sin \beta_j \dot{\theta}_1) / (\delta_j \rho_j)$, which leads to

$$\dot{\theta}_1 = \frac{Q_1}{2 \left(\frac{u_0 v_0 A_0 \sin \beta_0}{\delta_0 \rho_0} + \frac{u_1 v_1 A_1 \sin \beta_1}{\delta_1 \rho_1} \right)} \quad (17)$$

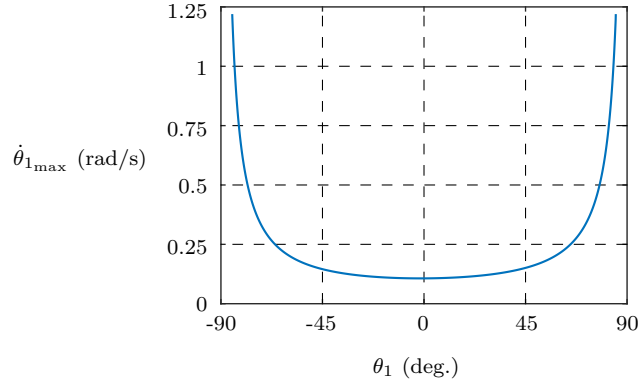


Fig. 6. Maximum angular velocity of the swing joint (*i.e.* $\dot{\theta}_{1\max}$) based on flow rate limitations in terms of its angular position θ_1

Table 1. Parameter values for a typical rockbreaker

i	a_i (m)	u_i (m)	v_i (m)	ε_i (deg)	$Q_{i\max}$ (L/min)	j	$\rho_{j\min}$ (m)	$\rho_{j\max}$ (m)	A_{blind_j} (m ²)	A_{rod_j} (m ²)
1	0.37	1.28	0.22	-89.04	24	0, 1	1.07	1.5	1.03×10^{-2}	7.16×10^{-3}
2	3.06	0.70	2.09	-57.63	60	2, 3, 4	1.54	2.65	2.01×10^{-2}	1.33×10^{-2}
3	2.38	2.07	0.73	-7.60	60					
4	2.57	2.12	0.63	60.56	38					

Setting $Q_1 = Q_{1\max}$, maximum permissible angular velocities of the swing joint (*i.e.* $\dot{\theta}_{1\max}$) may be obtained for corresponding joint positions (*i.e.* θ_1), the results of which are plotted in Fig. 6 for a typical rockbreaker. The swing joint velocity corresponding to the maximum valve flow rate increases dramatically close to the ends of its range of motion. This is due to a poor kinematic conditioning of the swing joint which makes the control of the rockbreaker's motion more difficult. For this reason, $\mathcal{C}_5: \theta_1 \leq \theta_{1\lim}$ is added as a constraint for the DSJM case where $\theta_{1\lim}$ is set to the lowest point on the $\dot{\theta}_{1\max}$ v. θ_1 plot. Since this plot contains a relative flat portion spanning the majority of the swing joint's range of motion, this additional constraint does not overly impede the planning of time efficient trajectories.

4. RESULTS

Using the proposed methodology, validation trajectories are generated using suitable software (*e.g.* MATLAB®) for a typical rockbreaker that is representative of commercially available systems. In addition to $b = 1.10$ m, $\gamma = 5.20^\circ$ and $Q_{p\max} = 170$ L/min, the remaining parameter values that were used are presented in Table 1. Based on a typical underground rockbreaker installation, positions in the work plane located above each corner of a grizzly (refer to Fig. 1(a)) are defined in Table 2 along with their corresponding breaker orientations. It may be noted that vertical breaker orientations are not possible when the rockbreaker is located in the FL and FR positions such that the orientation closest to vertical, as identified using the approach illustrated in Fig. 4, has been used. From the poses listed in Table 2, the validation trajectories that were used are defined in Figure 1(b). Although the trajectory planning algorithms are not intended for real-time planning (*i.e.* planning occurs prior to rockbreaker motion), the typical delay in computing an optimized trajectory using either the DSJM or CSLM approach is approximately 50 ms or less once the code has been compiled to C.

For the case of T1, the x , y and z coordinates of the breaker tip position are plotted as a function of time for each path planning approach in Figs. 7(a) and 7(b). The difference between paths planned using the DSJM

Table 2. Rockbreaker poses used to define validation trajectories

	x (m)	y (m)	z (m)	ϕ (deg.)
Near left corner (NL):	2.20	2.15	-1	270
Near right corner (NR):	2.20	-2.15	-1	270
Far left corner (FL):	6.27	2.15	-1	293.6
Far right corner (FR):	6.27	-2.15	-1	293.6

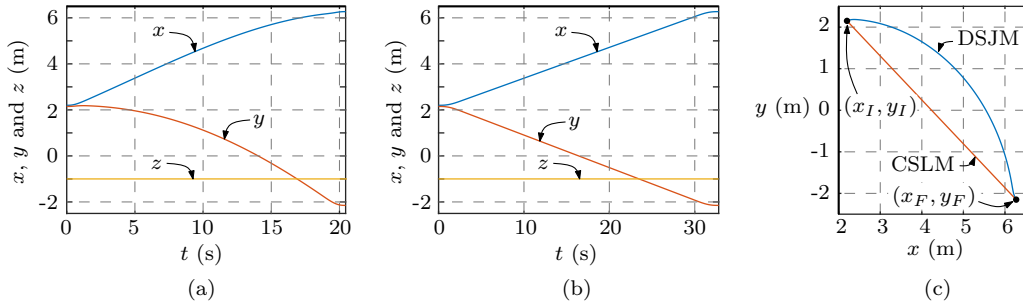


Fig. 7. Trajectory T1: Position of breaker tip as a function of time using (a) the DSJM approach and (b) the CSLM approach and (c) motion of the breaker tip within the X_1Y_1 plane.

and CSLM approaches become apparent in Fig. 7(c) where the respective trajectories are plotted in the X_1Y_1 plane. It would in fact appear that the CSLM approach is more efficient as the resulting path bringing the breaker tip from its initial to its final position is a straight line. However, the trajectory durations for the DSJM and CSLM approaches are 20.5 and 32.8 seconds, respectively. Looking at Figs. 8(a) and 8(b), the CSLM-based trajectory requires non-monotonous hydraulic actuator length fluctuations (*i.e.* ρ_3 and ρ_4). As these fluctuations represent an inefficient use of available valve and pump flow rates, they lead to an increased trajectory duration. Ultimately, the most time efficient trajectory in this regard would be obtained from a straight line path in the rockbreaker's actuator space (*i.e.* the hyperspace defined by the components of ρ). However, such an approach would make it very challenging to plan rockbreaker trajectories effectively as these are more naturally defined in its task space.

The optimized durations for T1 through T6, obtained using both the DSJM and CSLM approaches, are summarized in Table 3. The DSJM generally leads to shorter trajectory durations as it more closely replicates

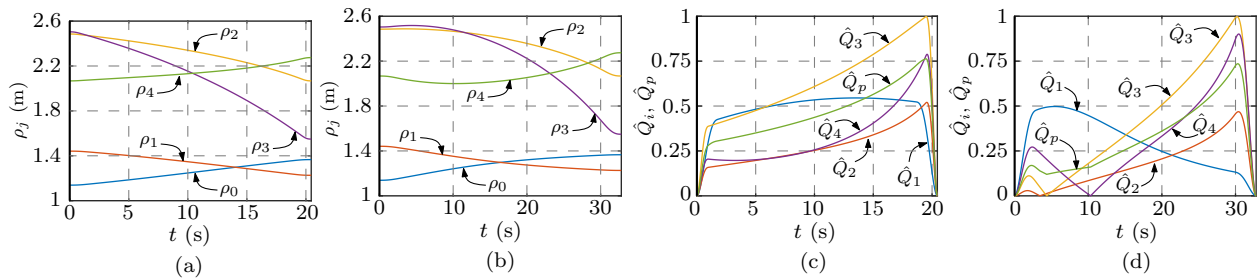


Fig. 8. Trajectory T1: Hydraulic actuator lengths for the (a) DSJM and (b) CSLM approaches and normalized flow rates for the (c) DSJM and (d) CSLM approaches.

Table 3. Comparison of trajectory durations obtained using the DSJM and CSLM approaches.

Trajectories:		T1	T2	T3	T4	T5	T6
t_f (sec.)	DSJM	20.5	30.9	20.5	30.9	15.5	7.1
	CSLM	32.8	50.0	22.7	34.7	19.3	15.9

the time-optimal straight line in actuator space. However, both approaches bring value to the trajectory planning process since one is guaranteed to remain in the rockbreaker workspace (useful to ensure feasible trajectories) while the other is guaranteed to remain in a region situated directly above the grizzly (useful for collision avoidance with nearby wall or rock faces). Referring to Fig. 1(a) and Fig. 1(b), one may observe that T1 and T2, for instance, connect the same two breaker positions in an alternating sequence (the same could be said for T3 and T4). However, as seen in Table 3, the durations of these trajectories based on the DSJM approach are not equal. This is explained by the difference in the rod and blind side surface areas of a hydraulic actuator's piston, which imply that a greater flow rate is required during the actuator's extension at a given rate than during its retraction. This influences the trajectory optimization through constraint \mathcal{C}_4 . Meanwhile, it may be observed that the durations of T1 and T3 (or T2 and T4) using the DSJM approach are equal. This result, which may initially appear as non-intuitive, is explained by the fact that both trajectories require the same motion to take place within the X_2Y_2 plane. Since, for these trajectories, the motion in this plane is more time consuming than the swing joint motion, it dictates the overall trajectory duration. As such, though the swing joint motion of T1 and T3 (or T2 and T4) are different, they do not influence the trajectory duration.

Finally, the normalized flow rates through each of the rockbreaker's proportional valves, *i.e.* $\hat{Q}_i = Q_i/Q_{i_{\max}}$ ($i = 1, 2, 3, 4$), as well as the normalized flow rate through its hydraulic pump, *i.e.* $\hat{Q}_p = Q_p/Q_{p_{\max}}$, are plotted in Figs. 8(c) and 8(d) for T1. The effectiveness of constraint \mathcal{C}_4 in terms of ensuring that the rockbreaker's flow rate limits are always respected may be observed. In both the DSJM and CSLM approaches, the proportional valve driving the hydraulic actuator of length ρ_3 is responsible for limiting the optimization of the trajectory duration. In terms of comparison, the DSJM approach requires a total flow of 26.2 L from the hydraulic pump during T1 while in the case of the CSLM approach this is 29.0 L.

5. DISCUSSION AND CONCLUSION

A trajectory planning methodology has been developed for use in a semi-automated rockbreaker system. DSJM and CSLM path planning approaches were proposed. In each case, the breaker is maintained as close as possible to a vertical orientation while its tip is kept in a horizontal work plane located above the ore pile. The DSJM approach guarantees that the path followed by the rockbreaker remains within its workspace. However, the breaker tip is not guaranteed to remain directly above the grizzly, which increases the likelihood of collisions. The issue is addressed by the CSLM approach but it may lead to paths that travel outside the rockbreaker's workspace. The time parameterization of the DSJM and CSLM paths uses a trajectory profile consisting of polynomial ramp-up/down trajectory segments leading to/from a constant velocity segment. This profile is optimized to minimize the trajectory duration while ensuring the satisfaction of valve and pump flow rate limits. It was found that the DSJM approach typically leads to trajectories of a shorter duration due to the decoupling of the swing joint motion.

Referring to Figs. 8(c) and 8(d), one may observe that the flow rate limits are only reached at a specific point along the trajectory (at $t = 19.5$ seconds in Fig. 8(c) and $t = 30.2$ seconds in Fig. 8(d)). In contrast, when operated by humans, the rockbreaker's valves are often opened to their full capacities during large portions of its motion. With this in mind, future work will seek to improve the trajectory planning methodology to better exploit the flow rate capacities so as to better approximate the transit times achieved by human

operators while ensuring the smooth and predictable operation of the rockbreaker.

ACKNOWLEDGEMENTS

This work was supported by the Centre for Excellence in Mining Innovation (CEMI) through the Ultra-Deep Mining Network (UDMN) program.

REFERENCES

1. Boeing, A. "A remotely operated robotic rock breaker with collision avoidance for the mining industry." In "Proceedings of the 30th International Symposium on Automation and Robotics in Construction and Mining," pp. 875 – 884. Montreal, QC, Canada, 2013.
2. Chang, P.H. and Lee, S.J. "A straight-line motion tracking control of hydraulic excavator system." *Mechatronics*, Vol. 12, No. 1, pp. 119 – 138, 2002.
3. Chacko, V., Yu, H., Cang, S. and Vladareanu, L. "State of the art in excavators." In "Proceedings of the International Conference on Advanced Mechatronic Systems," pp. 481 – 488. Kumamoto, Japan, 2014.
4. Corke, P., Roberts, J., Cunningham, J. and Hainsworth, D. *Springer Handbook of Robotics*, chap. Mining Robotics, pp. 1127–1150. Springer, 2008.
5. Bernold, L.E. "Quantitative assessment of backhoe operator skill." *Journal of Construction Engineering and Management*, Vol. 133, No. 11, pp. 889 – 899, 2007.
6. Duff, E., Caris, C., Bonchis, A., Taylor, K., Gunn, C. and Adcock, M. "The development of a telerobotic rock breaker." *Springer Tracts in Advanced Robotics*, Vol. 62, pp. 411 – 420, 2010.
7. Morales, D.O., Westerberg, S., La Hera, P.X., Mettin, U., Freidovich, L. and Shiriaev, A.S. "Increasing the level of automation in the forestry logging process with crane trajectory planning and control." *Journal of Field Robotics*, Vol. 31, No. 3, pp. 343–363, 2014.
8. Jeevamalar, J. and Ramabalan, S. "Optimal trajectory planning for autonomous robots - A review." In "Proceedings of the 1st International Conference on Advances in Engineering, Science and Management," pp. 269–275, 2012.
9. Ratiu, M. and Adriana Prichici, M. "Industrial robot trajectory optimization - A review." In "Annual Session of Scientific Papers IMT ORADEA," Vol. 126, 2017.
10. Xu, J. and Yoon, H.S. "A review on mechanical and hydraulic system modeling of excavator manipulator system." *Journal of Construction Engineering*, 2016.
11. Stentz, A., Bares, J., Singh, S. and Rowe, P. "Robotic excavator for autonomous truck loading." *Autonomous Robots*, Vol. 7, No. 2, pp. 175–186, 1999.
12. Kim, Y.B., Ha, J., Kang, H., Kim, P.Y., Park, J. and Park, F.C. "Dynamically optimal trajectories for earthmoving excavators." *Automation in Construction*, Vol. 35, pp. 568–578, 2013.
13. Lee, B. and Kim, H.J. "Trajectory generation for an automated excavator." In "Proceedings of the 14th International Conference on Control, Automation and Systems," pp. 716–719. IEEE Computer Society, 2014.
14. Zhang, B., Wang, S., Liu, Y. and Yang, H. "Research on trajectory planning and autodig of hydraulic excavator." *Mathematical Problems in Engineering*, Vol. 2017, 2017.
15. Lynch, K.M. and Park, F.C. *Modern Robotics: Mechanics, Planning and Control*. Cambridge University Press, 2017.
16. Craig, J.J. *Introduction to robotics: Mechanics and control*. Fourth ed.. Pearson, 2017.
17. Tremblay, L.F., Arsenault, M. and Zeinali, M. "Simplification of the dynamic model of a hydraulic rockbreaker for implementation in a model-based control scheme." *Transactions of the CSME*, Vol. 42, No. 1, pp. 38–48, 2018.